ROYAL SOCIETY
OF CHEMISTRY

PAPER

Check for updates

Synthesis and structural design of microspheres comprising cellulose nanofibers and artificial lignin polymer by enzyme-mediated Pickering emulsion templating†

Yuna Tanaka,‡ Qi Li, [ID] ‡ Mayumi Hatakeyama [ID] and Takuya Kitaoka [ID] *

With the rapid advancement of plastics, microparticles and microbeads are becoming an integral part of various applications such as detergents, cleaning products, and cosmetics. This has resulted in the severe and irreversible contamination of ecosystems, especially the marine environment. Woody polysaccharides and lignin are biodegradable and can be decomposed by marine microorganisms. In the present study, we synthesized an artificial lignin polymer (ALP) that was densely enveloped in cellulose nanofibers (CNFs) by enzyme-mediated Pickering emulsion templating. We used isoeugenol, which is a structural analogue of lignin precursors, as the oil phase, and either native CNFs or CNFs surface-modified with carboxy, sulfate, or phosphate groups as Pickering emulsion stabilizers. Dehydrogenative polymerization was initiated by horseradish peroxidase and hydrogen peroxide. The resulting microspheres were 1–2 μm in diameter and had a sphericity of more than 98%. The yield was high (51–81%). Scanning electron microscopy and toluidine blue staining revealed that the shell layers of the microspheres comprised dense nanofiber networks of various CNFs, whereas the core components comprised a β-5-rich lignin-like structure, as determined by nuclear magnetic resonance analysis. We monitored the pH-dependent adsorption and desorption behaviors of the toluidine blue dyes, which changed according to the functional groups introduced on the native CNF. This facile strategy will enable the development of versatile and sustainable microparticles enveloped in CNFs, which are potentially useful as marine-biodegradable cosmetic microparticles.

Sustainability spotlight

Environmental pollution and health risks caused by microplastics and microbeads have received marked attention in recent years. The development of sustainable biodegradable and biocompatible microparticles is key to preventing marine pollution by microplastics. This must be achieved by replacing plastics derived from fossil fuels with environmentally benign biomaterials. The present work provides a greener strategy for the synthesis of artificial lignin polymers enveloped with cellulose nanofibers by an enzyme-mediated Pickering emulsion templating method. It will facilitate the greater use of renewable, carbon dioxide-fixed woody nanomaterials in cosmetics. This simple strategy reduces dependence on fossil fuels and aligns with the SDGs 12 (responsible consumption and production), 13 (climate action), 14 (life below water), and 15 (life on land).

Introduction

Microparticles that are derived from cosmetic microbeads or the degradation of plastics have received marked global attention owing to their undeniable environmental impact and the potential risks that they pose to human health.[1,2] Because many plastic products are single-use and difficult to degrade, 79% of plastic pollution accumulates in ecosystems.[3] Moreover, it is predicted that approximately 53 million metric tons of plastic waste will enter aquatic ecosystems annually by 2030.[4] According to the latest data, over 170 trillion plastic particles are floating in the world's oceans. The fragmentation of plastics causes the formation of secondary microparticles that eventually enter shoreline and seafloor compartments, resulting in latent damage to organisms through ingestion.[2,5] Microbeads, which are widely used in cosmetic products, have also caused severe contamination of the marine environment, threatening both aquatic animals and humans.[6] The replacement of petroleum-based microplastics or microbeads with sustainable and biodegradable biomaterials will significantly improve the marine environment. Recently, bio-based polysaccharides such

Department of Agro-Environmental Sciences, Graduate School of Bioresource and Bioenvironmental Sciences, Kyushu University, Fukuoka 819-0395, Japan. E-mail: tkitaoka@agr.kyushu-u.ac.jp

as cellulose, chitin, and chitosan have been investigated as new candidates for the construction of green microparticles owing to their abundance, excellent biocompatibility, and biodegradability.[7,8] Cellulose, which is the major skeletal component of plants and trees, and is the most abundant biomacromolecule in nature, is particularly attractive for various applications, including drug delivery, personal care products, and cosmetics.[9,10] In addition to terrestrial fungi and bacteria, a salt-tolerant enzyme with glucosidase activity has been found in marine bacteria such as *Croceicoccus marinus*, suggesting that they may be responsible for the degradation of cellulose in the marine environment.[11] Lignin, another major component of plants and trees, is also abundant in nature, and biodegrades on land and in water, where marine lignin-degrading bacteria have recently been discovered.[12] Therefore, wood-based microparticles composed of cellulose and lignin hold the key to the development of renewable and eco-friendly cosmetic products.

Cellulose nanofibers (CNFs), which are derived from wood and cotton, are typically ∼3 nm wide, have a high aspect ratio, and designable surface functionality. They are therefore suitable for various applications, including cosmetics, biomedical materials, electronics, and food packaging.[13–15] In addition to its high aspect ratio, the naturally occurring amphiphilic surface of CNF makes it suitable as a novel Pickering emulsion (PE) stabilizer.[16] CNF-based PE systems are exceptionally stable with regard to coalescence, temperature, and pH changes, indicating their potential usefulness in applications such as food and cosmetics.[17,18] However, owing to the hydrophilicity of CNFs and their tendency to form strong networks by hydrogen bonding, well-dispersed CNFs are difficult to obtain in most non-polar polymer matrices.[19] Alternatively, surface modification such as polymer/molecule grafting or adsorption can be applied to improve the dispersibility and compatibility of CNFs.[20] Chemical modifications, including carboxylation, sulfation, and phosphorylation, have been developed to impart specific properties to nanocellulose (collective name for cellulosic nanomaterials), and further extend its usefulness in demanding applications.[21] 2,2,6,6-Tetramethylpiperidine-1-oxyl (TEMPO)-oxidized CNF (TOCNF) with carboxylate groups has been used to stabilize a divinylbenzene/water-type PE and construct core–shell microparticles by *in situ* radical polymerization.[22] However, cores comprising polydivinylbenzene are completely non-biodegradable in nature. Therefore, the construction of biodegradable microparticles for cosmetic applications by cellulose-based PE templating is of great significance.

Cellulose-based microparticles have been investigated for drug delivery and sustainable release *via* spray-drying.[23–25] Furthermore, cellulose aerogel microparticles with large specific surface areas have been constructed by emulsion-coagulation methods.[26] In our previous studies, we used nanocellulose-stabilized PEs containing coniferyl alcohol to obtain hydrophobic dehydrogenative polymers (DHPs), which formed at the oil–water interface.[27] The DHPs were successfully synthesized in the presence of TOCNF *via* a one-pot, one-step aqueous process without any organic solvents, resulting in the formation of particles of several hundred nanometers in size, which were smaller than those required in cosmetics.[28] Lignin

nanoparticles have been produced by spray-drying methods; however, the use of black powders in cosmetic applications is limited.[29] Therefore, the fabrication of microparticles by using various CNFs and non-black lignin remains challenging.

We used four types of CNFs as PE stabilizers in the present work: native CNF, TOCNF, sulfated CNF (S-CNF), and phosphorylated CNF (P-CNF). Isoeugenol (IE), which is a structural analogue of lignin precursors, was used as the oil phase to form stable PEs by ultrasonic homogenization. Notably, the degradation and conversion of IE have been confirmed in various microorganisms, especially in the genus *Psychrobacter* sp. CSW4 isolated from the sea water of the Caspian Sea.[30] This would contribute to the biodegradability potential of the final products obtained from the IE and CNFs. We investigated the morphology and size of each type of nanofiber and the corresponding PE. Horseradish peroxidase (HRP) and hydrogen peroxide (H_2O_2) were mixed with each PE to initiate the dehydrogenative polymerization of IE, and the pale yellow artificial lignin polymer (ALP) was synthesized inside the PE microparticles. We used scanning electron microscopy to examine the morphology of the nanocellulose in the shell layer, and determined the yield and the sphericity of the particles in each sample. The adsorption/desorption behavior of toluidine blue O (TBO) was also investigated to evaluate the functionality of the ALP/CNF microparticles. The present study provides a more sustainable and eco-friendly strategy that will facilitate the use of CNFs in ALP construction in the cosmetic industry.

Experimental

Materials

Wood-derived, physically nanopulverized commercial CNF (BiNFi-s, AFo-10002, 2.0% (w/w)) was purchased from Sugino Machine Ltd (Uozu, Japan), TOCNF (RHEOCRYSTA, I-2SX, 2.3% (w/w), carboxy content: 1.55 mmol g^{-1}, DKS Co. Ltd, Kyoto, Japan), S-CNF (research sample, sulfate content: 1.70 mmol g^{-1}, Yokogawa Bio Frontier Inc., Tokyo, Japan), and P-CNF (trial product, phosphate content: 1.48 mmol g^{-1}, Oji Holdings Corp., Tokyo, Japan) were kindly provided by the respective suppliers. Isoeugenol (IE, oil, purity >97% (GC)) was purchased from Tokyo Chemical Industry Co. Ltd (Tokyo, Japan). Horseradish peroxidase (HRP) and hydrogen peroxide (H_2O_2, 30% aqueous solution) were purchased from FUJIFILM Wako Pure Chemical Industries Ltd (Osaka, Japan). Other chemicals and solvents were obtained from Sigma-Aldrich Japan, Ltd (Tokyo, Japan), FUJIFILM Wako Pure Chemical Industries, Ltd (Osaka, Japan), and Tokyo Chemical Industry Co., Ltd (Tokyo, Japan). All chemicals were used as received without further purification. Water used in the present study was purified using a Barnstead Smart2Pure system (Thermo Scientific Co. Ltd, Tokyo, Japan).

Characterization of the CNF samples

The nanofiber morphologies of the unmodified original CNF and surface-modified CNFs were determined by transmission electron microscopy (TEM) at the Ultramicroscopy Research

Center, Kyushu University using a JEM-2100HCKM microscope (JEOL Ltd, Tokyo, Japan) operated at an accelerating voltage of 200 kV. Each CNF suspension (0.001–0.01 wt%, 3 μL) was dropped onto a copper grid (elastic carbon coated, ELS-C10, Okenshoji Co. Ltd, Tokyo, Japan) and dyed with 1% sodium phosphotungstate (3 μL) prior to TEM investigation. The nanofiber samples were also examined using an atomic force microscopy (AFM) system (Dimension Icon, Bruker Japan Co. Ltd, Tokyo, Japan) equipped with an RTESP-300 probe ($k = 40$ N m^{-1}, $F_0 = 300$ kHz) in tapping mode under ambient conditions. Each CNF suspension (0.005–0.01 wt%) was dropped onto a muscovite mica (V-1 grade, 01872-CA, Alliance Biosystems, Inc., Osaka, Japan), followed by air-drying. The average width of the CNFs was calculated from the height profiles of the AFM images ($n = 50$). The crystalline structures and crystallinity of the nanofiber samples were measured by X-ray diffraction (XRD) analysis. Diffraction profiles were obtained using a SmartLab diffractometer (Rigaku Corp., Tokyo, Japan) operated at 40 kV and 20 mA at the Center of Advanced Instrumental Analysis, Kyushu University. Ni-filtered Cu Kα radiation ($\lambda = 0.15418$ nm) was used in reflection mode from 5° to 40° at a scan rate of 2° min^{-1} with 0.01° intervals. The crystallinity index (CrI) of each sample was calculated using the Segal method.[31] The zeta potential value of each nanofiber suspension (0.01 wt%) was determined using a Zetasizer Nano ZS system (Malvern Panalytical, Tokyo, Japan).

Preparation and enzymatic polymerization of Pickering emulsions

Each Pickering emulsion was prepared from an oil substrate (IE, 0.5 mL, 3.3 mmol) and an aqueous CNF dispersion (0.4 wt%, 4.5 mL) by ultrasonic homogenization at room temperature for 60 s. This was followed by HRP-mediated polymerization: "bulk" polymerization, i.e., Zulaufverfahren (ZL), and "stepwise" polymerization, i.e., Zutropfverfahren (ZT) methods, both of which are well-known protocols for DHP synthesis.[32,33] In the case of the ZL method, as-prepared PE (5 mL) was diluted with phosphate buffer (pH 6.5, 10 mM, 20 mL) in which HRP (1 mg) was dissolved, and then allowed to stand at 37 °C for 48 h. Hydrogen peroxide (3%, 1.65 mL, 1.5 mmol) was added in two parts to the mixture at $t = 0$ and 24 h. In the ZT method, as-prepared PE (5 mL) was diluted with phosphate buffer (pH 6.5, 10 mM, 20 mL) containing HRP (1 mg), and then gently agitated at 37 °C for 48 h. Hydrogen peroxide (3%, 1.65 mL, 1.5 mmol) was gradually added to the mixture at a rate of 34.3 μL h^{-1}. When the polymerization was complete, the as-prepared microparticles were washed thoroughly with pure water, and centrifuged at 8500g for 3 min. The microparticles were then collected by lyophilization. The preparation procedure is summarized in Fig. 1.

Characterization of the emulsions and microparticles

A drop of each emulsified sample (3 μL) was placed on a glass slide and gently covered with a coverslip for examination using an optical microscope (DMI 4000B, Leica, Wetzlar, Germany). The droplet size was measured using a dynamic light scattering particle size analyzer (nanoPartica SZ-100, Horiba, Ltd, Kyoto, Japan). Each emulsion was diluted 10 times and poured into a quartz cell for the measurement. The same procedures were used to measure the microparticles. A water suspension of approximately 1% fine particles was poured into a quartz cell. To measure the zeta potential of the microparticles, a water suspension of microparticles (ca. 0.04%) was placed in a folded capillary cell and analyzed using a Zetasizer light scattering device (Zetasizer Nano ZS, Malvern Panalytical, Tokyo, Japan). The microparticles were investigated by scanning electron
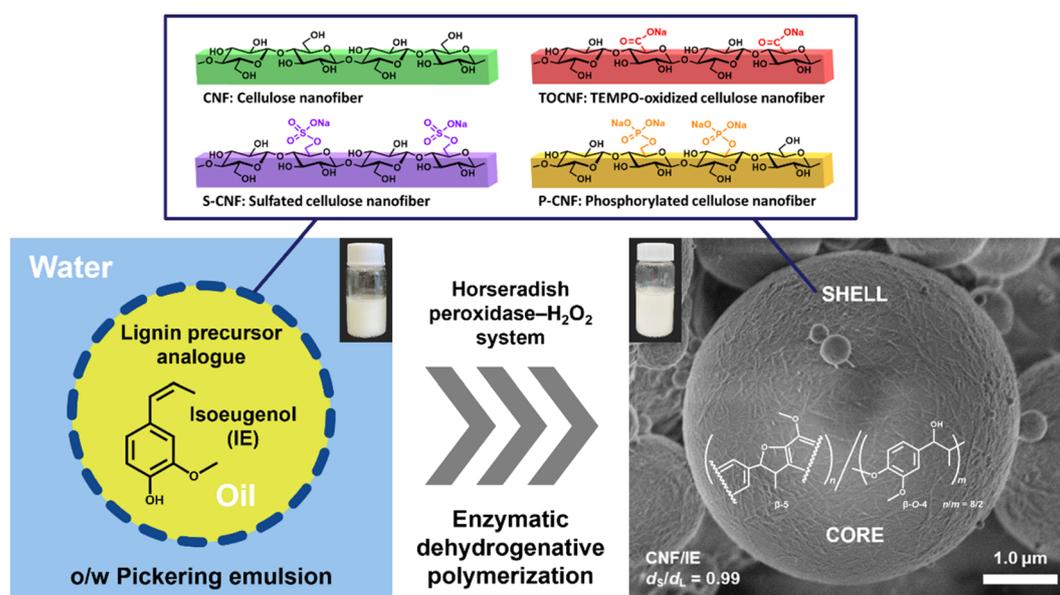

Fig. 1 Schematic illustration and SEM image of the enzymatic synthesis of artificial lignin polymer (dehydrogenative polymer of IE) microparticle as a core enveloped with CNF as a shell. (SEM = scanning electron microscopy; IE = isoeugenol; CNF = cellulose nanofiber).

microscopy (SEM). Each sample was suspended in water, dropped onto a carbon tape, and dried in a desiccator. The sample was then coated with an osmium coater (HPC-1SW, Vacuum Devices Corporation, Vacuum Devices, Inc., Ibaraki, Japan) for 2 s (ca. 3 nm thickness) and investigated using an ultra-high-resolution field-emission scanning electron microscope (SU8000, Hitachi High-Tech Corporation, Tokyo, Japan) at an acceleration voltage of 1 kV. Sphericity was expressed as a percentage by dividing the minor axis (d_S) by the major axis (d_L) of the particles obtained from the SEM images ($d_S/d_L \times 100$).

Analytical characterization of as-synthesized ALPs

As-prepared microparticles were dissolved in ethanol, and the supernatant (CNF-free ALP fractions) obtained after centrifugation ($10\,000g$, 3 min) was used for matrix-assisted laser desorption/ionization−time-of-flight mass spectrometry (MALDI TOF-MS). The ionization matrix was 2,5-dihydroxybenzoic acid. The measurements were obtained using a MALDI TOF-MS system (AXIMA® Performance, Shimadzu Corporation, Kyoto, Japan) in reflectron mode. In a similar way, the collected ALP fractions were dried under reduced pressure to remove the solvent and stored in a reduced-pressure desiccator. Each sample was then dissolved in deuterated chloroform ($CDCl_3$) and analyzed using an NMR system (JNM-ECS400, JEOL Ltd, Tokyo, Japan).

Toluidine blue O staining assay

As-prepared microparticles (ca. 36 mg) were dispersed in 3.6 mL of deionized water, 400 µL of TBO solution (100 mg L^{-1}) was added, and the color change indicating metachromasia was recorded with a digital camera. The adsorption/desorption behavior of the TBO on the microparticles was investigated. ALP/CNF microparticles (5 mg) were dispersed in TBO solution (pH 7.0, 10 mg L^{-1}, 500 µL) and allowed to stand for 3 min. Subsequently, 450 µL of the supernatant was collected by centrifugation ($10\,000g$, 3 min) (cycle 1). Phosphate buffer (pH 2.5 or pH 7.0, 10 mM, 450 µL) was added and the mixture was allowed to stand for 3 min. Subsequently, 450 µL of the supernatant was collected by centrifugation ($10\,000g$, 3 min) (cycle 2). The samples were washed with phosphate buffer (pH 2.5, 100 mM, 3 times), pure water (1 time), and phosphate buffer (pH 7.0, 10 mM, 1 time) in that order. Cycles 1 and 2 were then repeated (cycles 3 and 4). The collected supernatant was aliquoted into a 96-well plate, and the absorbance was measured at 595 nm using a microplate reader (iMark™ Microplate Reader, Bio-Rad Laboratories, Hercules, CA, USA).

Sun protection factor measurement

The sun protection factor (SPF) indicates UVB (280−320 nm) absorption performance, and indicates the level of suppressing sunburn and tanning in human skin. An SPF value of 50+ is the maximum for UVB protection. The SPF values of the ALP/CNF microparticles were determined using a UV-2000S Ultraviolet Transmittance Analyzer (Labsphere Inc., NH, USA). The measurement method was performed according to the

procedure described in the instruction manual of the device. The details of the sample and preparation method are described in Table S1 (ESI).†

Statistical analysis

All quantitative data are expressed as the mean ± SD, and were analyzed using OriginPro 2022b software (OriginLab Corp., Northampton, MA, USA). We considered p-values of <0.05 or <0.01 to indicate statistical significance.

Results and discussion

Structural characterization of the CNFs

We obtained AFM images (Fig. 2) and TEM images (Fig. S1†) that reveal the morphologies of the various CNFs examined in the present work: native CNF, TOCNF, S-CNF, and P-CNF. These CNFs exhibited very thin and long nanofiber shapes with high aspect ratio and had entangled network structures, whereas the S-CNF possessed a rod-like morphology. The average width of the native CNF was ∼6.6 nm and its crystallinity was 85.3%. The average widths of the surface-modified CNFs varied from 2 to 3 nm on an inherent scale, and thus they were much thinner than the native CNF. After surface modification, the crystallinity of the CNFs decreased (61.8% for the TOCNF, 38.8% for the S-CNF, and 40.9% for the P-CNF), whereas the absolute zeta potential values increased, as listed in Table 1. The improved zeta potential values indicated the better dispersibility and stability of the surface-modified CNF suspensions. Table 1 summarizes the size and properties of each type of nanofiber.

Sizes and morphologies of the PEs and ALP/CNF microparticles

The PEs were prepared from native CNF or surface-modified CNFs via sonication. The solid content of the nanofiber suspension was fixed at 0.4 wt% and the oil phase ratio was 10%. An emulsion stabilized with 0.1% sodium dodecyl sulfate (SDS) was used as a control sample. As shown in Fig. 3a, the droplet sizes of the nanocellulose-stabilized PEs varied from 3.5 to 5.4 µm, whereas the control sample had a smaller droplet size of ∼1.1 µm. After storage at 37 °C for 48 h, the droplet sizes of the PEs increased slightly. However, the optical images confirmed the uniform morphology of the PEs microparticles, indicating excellent stability. This can be explained by the irreversible adsorption of the flexible nanofibers onto the oil–water interface, forming a network structure around the emulsion droplets, which increased the steric hindrance and inhibited the free movement of the droplets.[16,34] To obtain ALP/CNF microparticles, the PEs were diluted with buffer containing HRP, and hydrogen peroxide was added to conduct enzymatic dehydrogenative polymerization. The morphologies and digital images at each step are shown in Fig. 3b. The droplet sizes of the samples at each step are shown in detail in Fig. S2.† During polymerization, the surface-modified CNFs maintained the emulsion stability, whereas the unmodified CNF exhibited severe phase separation, as shown in Fig. 3b. After lyophilization, the microparticles decreased in size to 1.2–1.7 µm; they
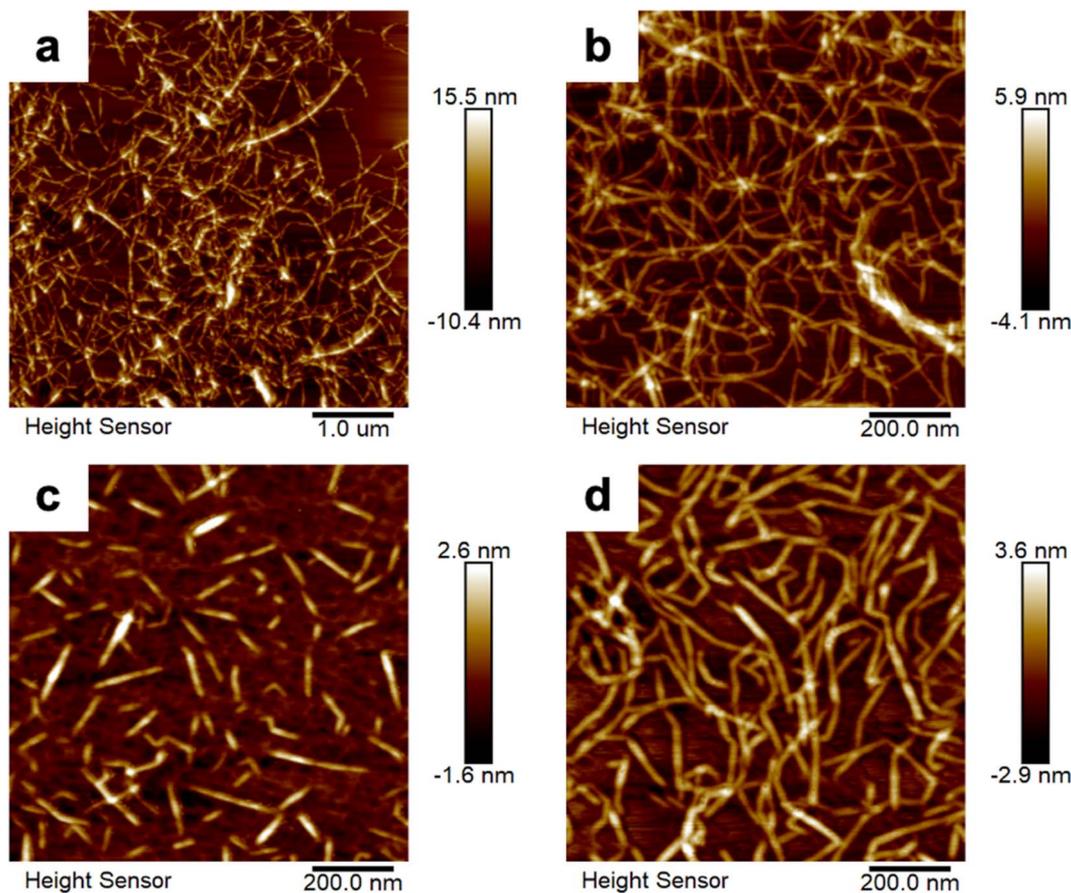
Fig. 2 AFM images of (a) CNF, (b) TOCNF, (c) S-CNF, and (d) P-CNF. (AFM = atomic force microscopy; CNF = cellulose nanofiber; TOCNF = 2,2,6,6-tetramethylpiperidine-1-oxyl (TEMPO)-oxidized CNF; S-CNF = sulfated CNF; P-CNF = phosphorylated CNF).

Table 1 Characterization of CNF and surface-modified CNFs[a]

Sample	Width (nm) mean ± SD	Crystallinity (%)	Zeta potential (mV) mean ± SD	Functional group (mmol g^{-1})
CNF	6.6 ± 1.9	85.3	−27.1 ± 3.6	—
TOCNF	2.1 ± 0.7	61.8	−53.6 ± 4.1	1.55
S-CNF	1.9 ± 0.5	38.8	−53.5 ± 7.1	1.70
P-CNF	2.7 ± 0.7	40.9	−51.1 ± 6.1	1.48

[a] CNF = cellulose nanofiber; TOCNF = 2,2,6,6-tetramethylpiperidine-1-oxyl (TEMPO)-oxidized CNF; S-CNF = sulfated CNF; P-CNF = phosphorylated CNF. The average width of the CNFs was calculated from the height profiles of the AFM images ($n = 50$).

had uniform droplet size distribution and coefficient of variance values around 20%, and were therefore suitable for commercial products. Owing to the rapid progression of polymerization, the self-assembly of the substrate exceeded the stability of the emulsion, resulting in the formation of smaller particles on the surfaces of the emulsion droplets.[35] Moreover, all the samples exhibited high sphericity of up to 98% as calculated from the SEM images (Fig. 4). Microparticle sphericity is an important indicator in cosmetic applications, and the obtained data fully satisfied that requirement. Nanofibrous materials were observed on and between ALP/CNF microparticles. In particular, the nanofiber structure of the shell layer is

clear in the enlarged SEM images (Fig. 4f), which confirm the successful synthesis of the core–shell structure *via* PE templating. As listed in Table 2, the ALP/CNF microparticles had sufficiently large negative zeta potentials, which ensured their stability in each suspension. The absolute values of the ALP/CNF microparticle surface-modified CNFs were much higher than those of the native CNF, suggesting the presence of dissociated functional groups on the surfaces of the ALP/CNF microparticles synthesized using TOCNF, S-CNF, and P-CNF. On the basis of these results, the obtained microparticles prepared by the polymerization of PEs containing 0.4 wt% CNFs would be suitable and safe for use as cosmetic additives.[36] The
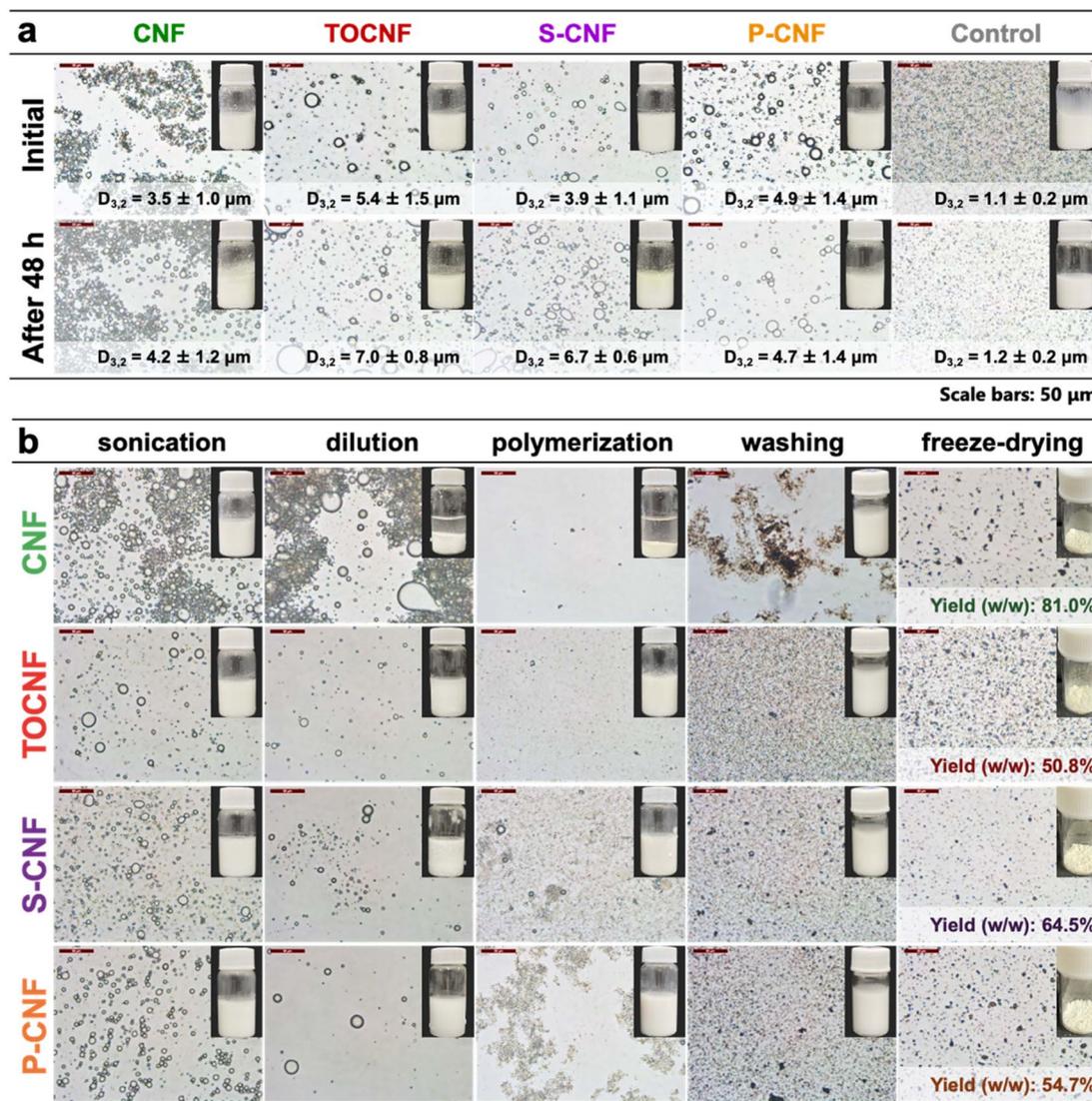
Fig. 3 Optical images of (a) PE samples stabilized with CNF, TOCNF, S-CNF, and P-CNF immediately after emulsification and after 48 h at 37 °C, and (b) PE and microparticles during the process of emulsification by sonication, dilution, polymerization, washing and freeze-drying. Scale bars: 50 μm. (PE = Pickering emulsion; CNF = cellulose nanofiber; TOCNF = 2,2,6,6-tetramethylpiperidine-1-oxyl (TEMPO)-oxidized CNF; S-CNF = sulfated CNF; P-CNF = phosphorylated CNF; control: ALP without CNFs).

ZL method produced a higher yield of ALP/CNF microparticles than the ZT method (CNF: 34.1%, TOCNF: 47.7%, S-CNF: 34.1%, and P-CNF: 62.2% including residual oil as unreacted IE). In addition, the ZT microparticles were distorted and fused together (Fig. S3†). Therefore, in the present work, we used the ZL method to construct the microparticles in the subsequent experiments. The data characterizing each ALP/CNF sample are summarized in Table 2. The size and surface morphology of the ALP/CNF microparticles were associated with the droplet size of the PE and could be regulated by controlling the polymerization conditions.

Structural analysis of the ALP/CNFs

We investigated the core structure of the microparticles in each sample using heteronuclear single quantum coherence nuclear magnetic resonance (HSQC-NMR) (Fig. 5) and MALDI TOF-MS (Fig. S4†). The peaks in the HSQC-NMR spectrum attributable to the unique β-O-4 and β-5 binding modes of lignin (Fig. 5) confirmed that the core comprised typical lignin-like chemical structures resulting from dehydrogenative enzymatic polymerization. Furthermore, comparing the integrated values of the α-position peaks attributable to the β-O-4 and β-5 linkages, the β-5 peak was approximately 4.4 times larger than the β-O-4 peak. This suggests that the cores of the ALP/CNF microparticles had a β-5-rich structure, which is consistent with the results of our previous study.[27] In particular, TOCNF exhibited the higher ratio of β-O-4 bond compared to other CNFs. Our previous study using TOCNF and organocatalysts in asymmetric aldol reactions has reported that the crystalline surface of TOCNF affects the binding mode of aromatic substrates, resulting in higher enantioselectivity.[37] The enzymatic dehydrogenative
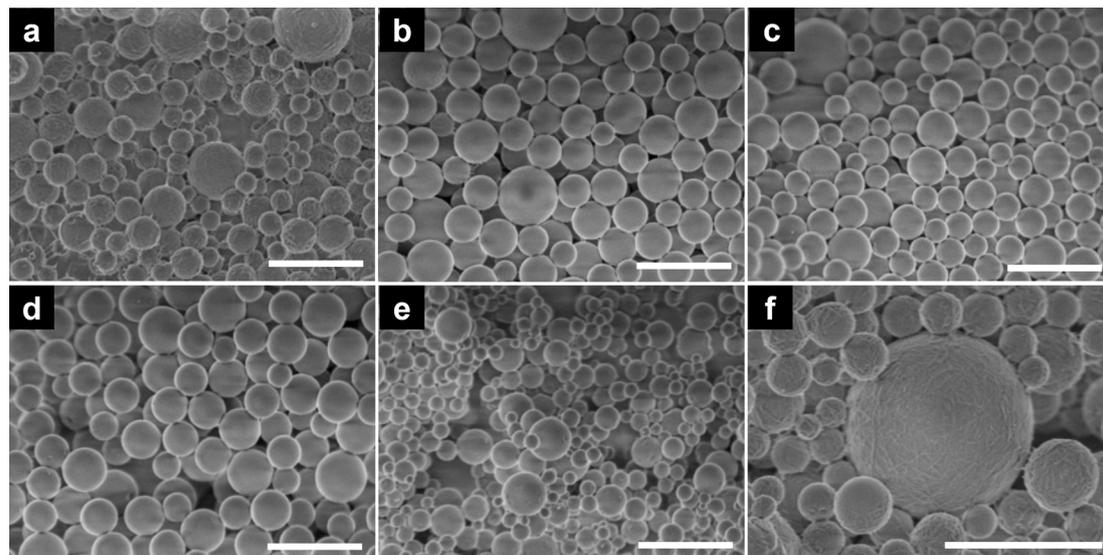
Fig. 4 SEM images of ALP microparticles enveloped with (a and f) CNF, (b) TOCNF, (c) S-CNF, (d) P-CNF, and (e) CNF-free (w/SDS control). Scale bars: 2 μm, acceleration voltage: 1.0 kV. (SEM = scanning electron microscopy; ALP = artificial lignin polymer; CNF = cellulose nanofiber; TOCNF = 2,2,6,6-tetramethylpiperidine-1-oxyl (TEMPO)-oxidized CNF; S-CNF = sulfated CNF; P-CNF = phosphorylated CNF; w/SDS = with sodium dodecyl sulfate).

Table 2 Characterization data of ALP/CNFs microparticles[a]

Sample	Particle size (μm) $D_{3,2}$ ± SD	Sphericity (%) d_S/d_L mean ± SD	Zeta potential (mV) mean ± SD	Yield (%) w/w
CNF	1.41 ± 0.29	98.6 ± 0.9	−36.9 ± 5.7	81.0
TOCNF	1.24 ± 0.25	98.3 ± 1.2	−47.3 ± 4.4	50.8
S-CNF	1.30 ± 0.26	99.1 ± 0.7	−51.2 ± 5.2	64.5
P-CNF	1.71 ± 0.37	99.1 ± 0.9	−47.8 ± 4.7	54.7
Control	1.10 ± 0.22	98.0 ± 1.7	−48.1 ± 5.4	30.2

[a] ALP = artificial lignin polymer; CNF = cellulose nanofiber; TOCNF = 2,2,6,6-tetramethylpiperidine-1-oxyl (TEMPO)-oxidized CNF; S-CNF = sulfated CNF; P-CNF = phosphorylated CNF; control: ALP without CNFs.

polymerization mechanism of IE in CNF-stabilized PE templating systems is currently unclear; however, the surface chemistry of the solid nanofiber stabilizers may play a significant role in the core formation of ALPs. When the degree of polymerization of the core was estimated by MALDI TOF-MS, we detected a series of 12 peaks with characteristic m/z intervals close to the molecular weight of the dehydrogenative monomer in the particles without a CNF coating using SDS, and a series of 8 peaks in the ALP/CNF microparticles, indicating the polymerization of IE (Fig. S4†). Although the possibility of insufficient ionization cannot be ruled out, a low degree of polymerization (up to an octamer) may provide an advantage when ALP/CNFs are considered for use in biodegradable cosmetics due to the biodegradability potential of natural lignin-like structure[12] and IE[30] in the sea.

Adsorption/desorption behavior of toluidine blue O

A facile strategy to confer various functionalities or enhance the efficacy of nanocellulose-based cosmetics is to adsorb other substances onto nanocellulose.[38] Therefore, we investigated the

adsorption/desorption behavior of TBO, which is a cationic dye, on ALP/CNF microparticles. According to the color difference shown in Fig. S5,† there was clear metachromasia from blue to violet on the surface-modified CNFs, although no color change occurred on the microparticles obtained using native CNF or SDS, indicating that the TBO dyes interacted with the dissociated acid groups on the surfaces of the ALP/surface-modified CNF microparticles. As shown in Fig. 6, the adsorption capacity of the microparticles obtained from surface-modified CNFs (TOCNF, S-CNF, and P-CNF) was much higher than that obtained from native CNF, which is consistent with Fig. S5.† An explanation for this is that surface modification by the introduction of carboxy, sulfate, or phosphate groups promoted electrostatic adsorption, whereas only physical adsorption may have occurred on the native CNF.[39,40] We investigated the desorption behavior of the ALP/CNF microparticles at pH 2.5 (Fig. 6a) and pH 7.0 (Fig. 6b). Notably, only ALP/CNFs that had been prepared with TOCNF or P-CNF exhibited obviously different desorption behavior, with complete desorption at pH 2.5. The difference in desorption behavior can be explained by
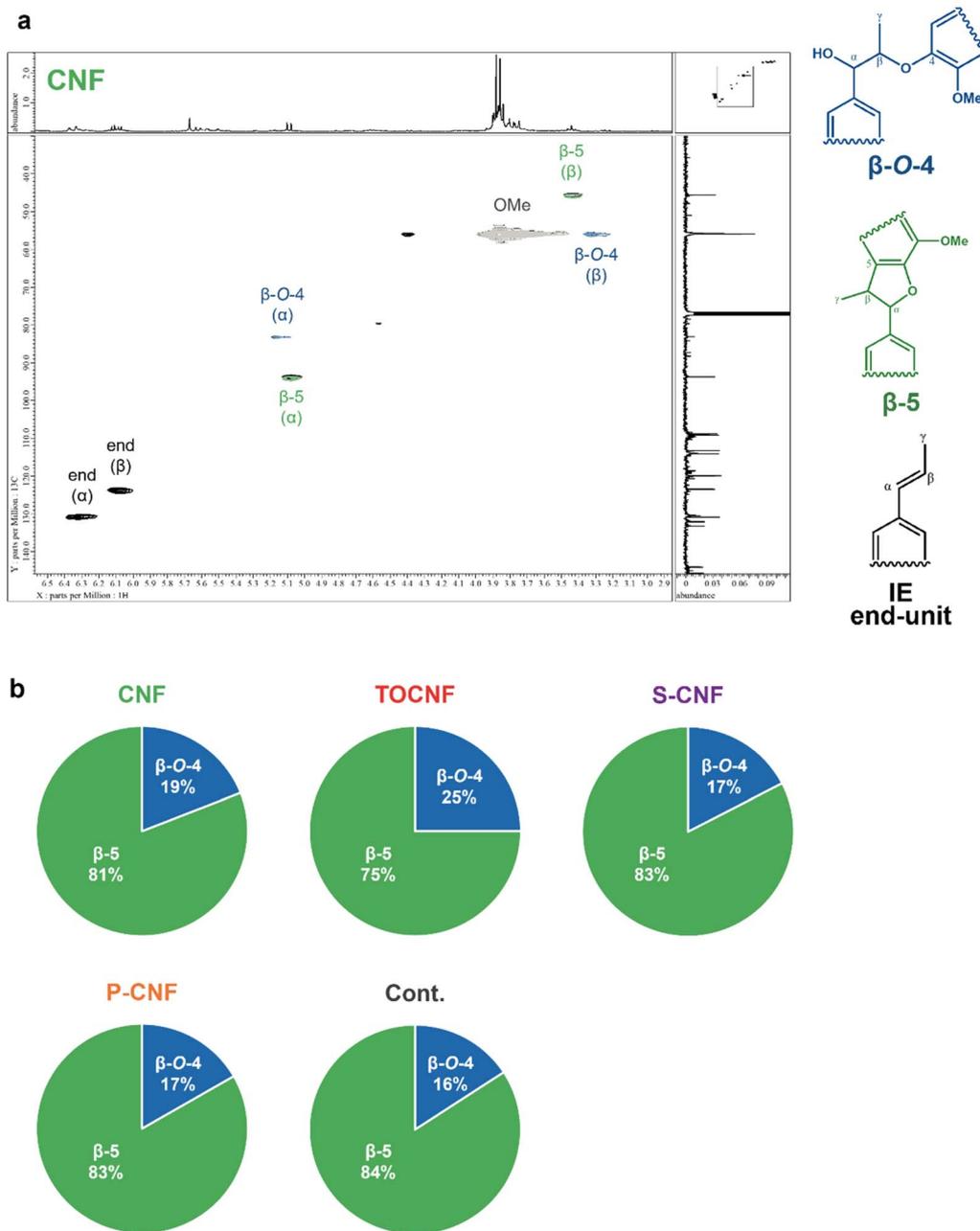
Fig. 5 (a) Typical HSQC-NMR spectrum of ALP/CNFs. (b) Ratio of binding modes of ALP fraction. Solvent: chloroform-*d* (deuterated chloroform). (HSQC-NMR = heteronuclear single quantum coherence nuclear magnetic resonance; ALP = artificial lignin polymer; CNF = cellulose nanofiber; TOCNF = 2,2,6,6-tetramethylpiperidine-1-oxyl (TEMPO)-oxidized CNF; S-CNF = sulfated CNF; P-CNF = phosphorylated CNF; IE = isoeugenol; cont.: ALP without CNFs).

the different pK_a values of each functional group: for TOCNF, the pK_a of the carboxy group is approximately 4–5; for P-CNF, the pK_{a1} and pK_{a2} are 3.1 and 8.3,[41] respectively; and for S-CNF, the pK_a of the sulfate group is less than 2.5.[42] Furthermore, the desorption capacity values of the ALP/P-CNF were approximately 30% in cycle 2 and 50% in cycle 4 at pH 7.0, which were larger than those of the ALP/TOCNF and ALP/S-CNF. These results confirm that the adsorption/desorption behavior can be regulated by pH and the surface functional groups of the CNFs enveloping the ALP core. Moreover, four cycles of

adsorption/desorption were successfully conducted using the same microparticles, which indicated promising reusability. Therefore, we anticipate that the ALP/CNF microparticles with uniform surface structures described herein will be useful for drug delivery systems and cosmetic products.

UV screening test for UVB absorption of the ALP/CNF microparticles

The SPF is an important indicator of UV screening because UVB (280–320 nm) is closely related to sunburn and tanning of
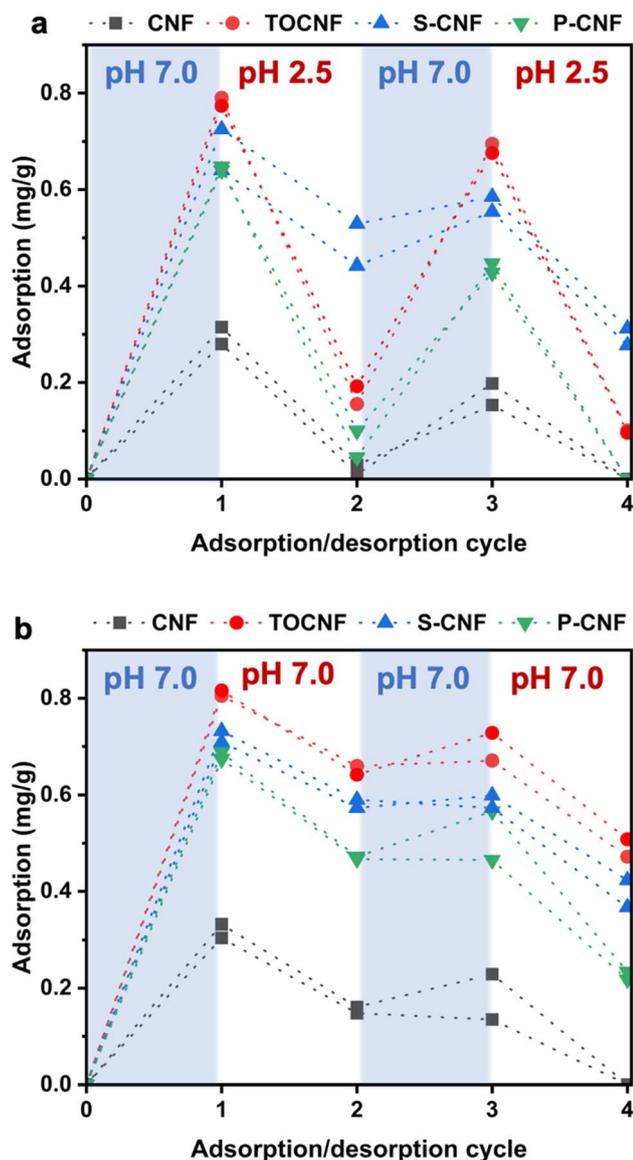
Fig. 6 Adsorption/desorption behavior of TBO to ALP/CNF microparticles. Cycles 1 and 3: adsorption at pH 7.0, cycles 2 and 4: desorption at (a) pH 2.5 or (b) pH 7.0. (TBO = toluidine blue O; ALP = artificial lignin polymer; CNF = cellulose nanofiber; TOCNF = 2,2,6,6-tetramethylpiperidine-1-oxyl (TEMPO)-oxidized CNF; S-CNF = sulfated CNF; P-CNF = phosphorylated CNF).

human skin.[43] Before testing the ALP/CNF microparticles, we determined the SPF value of our previously prepared microparticles constructed using TOCNF and cellulose diacetate.[44] The SPF value of a sample containing 5.0 wt% TOCNF/cellulose diacetate was approximately 21.4, which was almost the same as that of a particle-free basic cosmetic formulation. Following the addition of ALP/CNF microparticles, the SPF value of the sample increased markedly to 31.8, indicating significant UVB-blocking capability. Moreover, as shown in Fig. S6,† the microparticles were pale yellow (almost white) in color, which is desirable for cosmetic applications. In a previous study, the SPF value of pure NIVEA cream was increased to 15 following the addition of

10 wt% organosolv lignin.[45] The SPF values of sunscreen samples that contained 10 wt% of a partially or fully grafted alkali lignin-2-4-benzoyl-3-hydroxyphenyl acrylate copolymer were 18 and 59, respectively; however, the products were dark yellow in color.[46] Hence, the obtained results strongly indicated the potential for ALP/CNF microparticles in cosmetic products.

Conclusions

In the present study, we successfully synthesized wood-mimetic ALP microparticles that were densely enveloped in native CNF or surface-modified CNFs by enzyme-mediated PE templating. SEM images confirmed the spherical microparticles with a core–shell structure in which the shell layers were densely entangled with CNFs. The dehydrogenative polymerization of isoeugenol in an HRP–H_2O_2 system proceeded at the oil–water interface of the CNF-stabilized PE, resulting in the formation of pale yellow microspheres enveloped in a fine CNF network structure. CNFs that had been surface-modified with carboxylate, sulfate, or phosphate groups exhibited clear TBO metachromasia from blue to violet in aqueous suspensions, which indicated considerable reusability. These approximately octameric ALPs had β-5-rich structures, in contrast to conventional ALPs. The as-designed bio-based microparticles are spherical and UVB-absorbable, which makes them suitable for cosmetic applications, and their structures and properties are easily tuned. It is expected that such wood-mimetic microparticles comprising CNFs and ALPs will be biodegradable in the ocean, and their continuous use would contribute to an ecological and sustainable carbon cycle in ecosystems.

Data availability

The data that support the findings of this study are available from the corresponding author upon reasonable request.

Author contributions

Yuna Tanaka: data curation; formal analysis; investigation; visualization; writing – original draft. Qi Li: formal analysis; validation; visualization; writing – original draft. Mayumi Hatakeyama: formal analysis; validation; writing – review & editing. Takuya Kitaoka: conceptualization; methodology; funding acquisition; project administration; supervision; writing – review & editing. All authors agreed to take responsibility for all aspects of their work to ensure its integrity and accuracy.

Conflicts of interest

There are no conflicts to declare.

Acknowledgements

References

1 T. R. Walker and L. Fequet, *TrAC, Trends Anal. Chem.*, 2023, **160**, 116984.

2 M. Eriksen, W. Cowger, L. M. Erdle, S. Coffin, P. Villarrubia-Gómez, C. J. Moore, E. J. Carpenter, R. H. Day, M. Thiel and C. Wilcox, *PLoS One*, 2023, **18**, e0281596.

3 R. Geyer, J. R. Jambeck and K. L. Law, *Sci. Adv.*, 2017, **3**, e1700782.

4 S. B. Borrelle, J. Ringma, K. L. Law, C. C. Monnahan, L. Lebreton, A. McGivern, E. Murphy, J. Jambeck, G. H. Leonard, M. A. Hilleary, M. Eriksen, H. P. Possingham, H. De Frond, L. R. Gerber, B. Polidoro, A. Tahir, M. Bernard, N. Mallos, M. Barnes and C. M. Rochman, *Science*, 2020, **369**, 1515–1518.

5 V. N. de Ruijter, P. E. Redondo-Hasselerharm, T. Gouin and A. A. Koelmans, *Environ. Sci. Technol.*, 2020, **54**, 11692–11705.

6 Y. Zhou, V. Ashokkumar, A. Amobonye, G. Bhattacharjee, R. Sirohi, V. Singh, G. Flora, V. Kumar, S. Pillai, Z. Zhang and M. K. Awasthi, *Environ. Pollut.*, 2023, **320**, 121106.

7 C. A. King, J. L. Shamshina, O. Zavgorodnya, T. Cutfield, L. E. Block and R. D. Rogers, *ACS Sustainable Chem. Eng.*, 2017, **5**, 11660–11667.

8 J. Coombs OBrien, L. Torrente-Murciano, D. Mattia and J. L. Scott, *ACS Sustainable Chem. Eng.*, 2017, **5**, 5931–5939.

9 M. Miloloža, U. Rozman, D. Kučić Grgić and G. Kalčikova, *Chem. Biochem. Eng. Q.*, 2023, **37**, 181–188.

10 B. Robertson, L. Hoover, G. Rott, M. Quan and M. Calabrese, *Cellulose*, 2023, **30**, 8839–8859.

11 Y. Shen, Z. Li, Y.-Y. Huo, L. Bao, B. Gao, P. Xiao, X. Hu, X.-W. Xu and J. Li, *Front. Microbiol.*, 2019, **10**, 2922.

12 Y. Ley, X.-Y. Cheng, Z.-Y. Ying, N.-Y. Zhou and Y. Xu, *Microbiol. Spectrum*, 2023, **11**, e04424–22.

13 L. Amoroso, K. J. De France, C. I. Milz, G. Siqueira, T. Zimmermann and G. Nyström, *ACS Sustainable Chem. Eng.*, 2022, **10**, 342–352.

14 A. Isogai, *High-Performance and Specialty Fibers: Concepts, Technology and Modern Applications of Man-Made Fibers for the Future*, ed. The Society of Fiber Science and Technology, Japan, Springer, Tokyo, 2016, pp. 297–311.

15 A. Isogai and J. Fiber, *Sci. Technol.*, 2020, **76**, 310–326.

16 S. Fujisawa, E. Togawa and K. Kuroda, *Sci. Technol. Adv. Mater.*, 2017, **18**, 959–971.

17 L. Perrin, G. Gillet, L. Gressin and S. Desobry, *Polymers*, 2020, **12**, 2385.

18 Q. Li, Y. Wu, R. Fang, C. Lei, Y. Li, B. Li, Y. Pei, X. Luo and S. Liu, *Trends Food Sci. Technol.*, 2021, **110**, 573–583.

19 S. Kalia, S. Boufi, A. Celli and S. Kango, *Colloid Polym. Sci.*, 2014, **292**, 5–31.

20 F. Rol, M. N. Belgacem, A. Gandini and J. Bras, *Prog. Polym. Sci.*, 2019, **88**, 241–264.

21 Y. Habibi, *Chem. Soc. Rev.*, 2014, **43**, 1519–1542.

22 S. Fujisawa, E. Togawa, K. Kuroda, T. Saito and A. Isogai, *Nanoscale*, 2019, **11**, 15004–15009.

23 R. Kolakovic, T. Laaksonen, L. Peltonen, A. Laukkanen and J. Hirvonen, *Int. J. Pharm.*, 2012, **430**, 47–55.

24 Q. Qu, J. Zhang, X. Chen, H. Ravanbakhsh, G. Tang, R. Xiong, B. B. Manshian, S. J. Soenen, F. Sauvage, K. Braeckmans, S. C. De Smedt and C. Huang, *ACS Sustainable Chem. Eng.*, 2021, **9**, 387–397.

25 Z. Zhu, S. Fu and L. A. Lucia, *ACS Sustainable Chem. Eng.*, 2019, **7**, 5376–5384.

26 L. Druel, A. Kenkel, V. Baudron, S. Buwalda and T. Budtova, *Biomacromolecules*, 2020, **21**, 1824–1831.

27 K. Kanomata, N. Fukuda, T. Miyata, L. P. Y. Lam, T. Takano, Y. Tobimatsu and T. Kitaoka, *ACS Sustainable Chem. Eng.*, 2020, **8**, 1185–1194.

28 N. Fukuda, M. Hatakeyama and T. Kitaoka, *Nanomaterials*, 2021, **11**, 917.

29 Y. Peng, S. S. Nair, H. Chen, N. Yan and J. Cao, *ACS Sustainable Chem. Eng.*, 2018, **6**, 11078–11086.

30 M. Ashengroph, I. Nahvi, H. Zarkesh-Esfahani and F. Momenbeik, *Appl. Biochem. Biotechnol.*, 2012, **166**, 1–12.

31 L. Segal, J. J. Creely, A. E. Martin and C. M. Conrad, *Text. Res. J.*, 1959, **29**, 786–794.

32 K. V. Sarkanen, *Lignins: Occurrence, Formation, Structure and Reactions*, K. V. Sarkanen and C. H. Ludwig, ed. John Wiley & Sons, Inc., New York, 1971, p. 916.

33 B. Cathala, B. Saake, O. Faix and B. Monties, *Polym. Degrad. Stab.*, 1998, **59**, 65–69.

34 Q. Li, M. Hatakeyama and T. Kitaoka, *Adv. Funct. Mater.*, 2022, **32**, 2200249.

35 S. Fujisawa, E. Togawa and K. Kuroda, *Biomacromolecules*, 2017, **18**, 266–271.

36 S. M. Kim, E. Ji Gwak, S. H. Jeong, S. M. Lee, W. J. Sim and J. S. Kin, *J. Toxicol. Risk Assess.*, 2019, **5**, 029.

37 N. J. Ranaivoarimanana, X. Habaki, T. Uto, K. Kanomata, T. Yui and T. Kitaoka, *RSC Adv.*, 2020, **10**, 37064–37071.

38 A. Meftahi, P. Samyn, S. A. Geravand, R. Khajavi, S. Alibkhshi, M. Bechelany and A. Barhoum, *Carbohydr. Polym.*, 2022, **278**, 118956.

39 J. Araki, *Cellulose*, 2021, **28**, 7707–7715.

40 J. Araki and M. Nakajima, *Cellulose*, 2023, **30**, 849–855.

41 Y. Noguchi, I. Homma and T. Watanabe, *Cellulose*, 2020, **27**, 2029–2040.

42 O. V. Surov, A. V. Afineevskii and M. I. Voronova, *Cellulose*, 2023, **30**, 9391–9404.

43 Y. Matsumura and H. N. Ananthaswamy, *Toxicol. Appl. Pharmacol.*, 2004, **195**, 298–308.

44 Y. Tanaka, N. Fukuda, N. J. Ranaivoarimanana, M. Hatakeyama and T. Kitaoka, *BioResources*, 2023, **18**, 1482–1492.

45 Y. Qian, X. Zhong, Y. Li and X. Qiu, *Ind. Crops Prod.*, 2017, **101**, 54–60.

46 Y. Wu, Y. Qian, A. Zhang, H. Lou, D. Yang and X. Qiu, *Ind. Eng. Chem. Res.*, 2020, **59**, 17057–17068.